FULL PAPER

Dynamic Electromechanical Hydrogel Matrices for Stem Cell Culture

Han L. Lim, Jessica C. Chuang, Tuan Tran, Aereas Aung, Gaurav Arya,*
and Shyni Varghese*

Hydrogels have numerous biomedical applications including synthetic matrices for cell culture and tissue engineering. Here we report the development of hydrogel based multifunctional matrices that not only provide three-dimensional structural support to the embedded cells but also can simultaneously provide potentially beneficial dynamic mechanical and electrical cues to the cells. A unique aspect of these matrices is that they undergo reversible, anisotropic bending dynamics in an electric field. The direction and magnitude of this bending can be tuned through the hydrogel crosslink density while maintaining the same electric potential gradient, allowing control over the mechanical strain imparted to the cells in a three-dimensional environment. The conceptual design of these hydrogels was motivated through theoretical modeling of the osmotic pressure changes occurring at the gel-solution interfaces in an electric field. These electro-mechanical matrices support survival, proliferation, and differentiation of stem cells. Thus, these new three-dimensional in vitro synthetic matrices, which mimic multiple aspects of the native cellular environment, take us one step closer to in vivo systems.

1. Introduction

In living organisms, cells are generally surrounded by other cells and the extracellular matrix (ECM). Geometrical, chemical, mechanical, and electrical signals from the extracellular environment play a pivotal role in regulating cellular activities such as proliferation, migration, and differentiation.[1–5] Recapitulating such a multi-functional and dynamic micro-environment in an in vitro setting would have high impact in cell biology and medicine: it would provide an excellent model system for systematically dissecting cellular functions, signaling pathways, disease progression, and tissue morphogenesis

and also provide an in vitro system for regenerating functional cells and tissues.
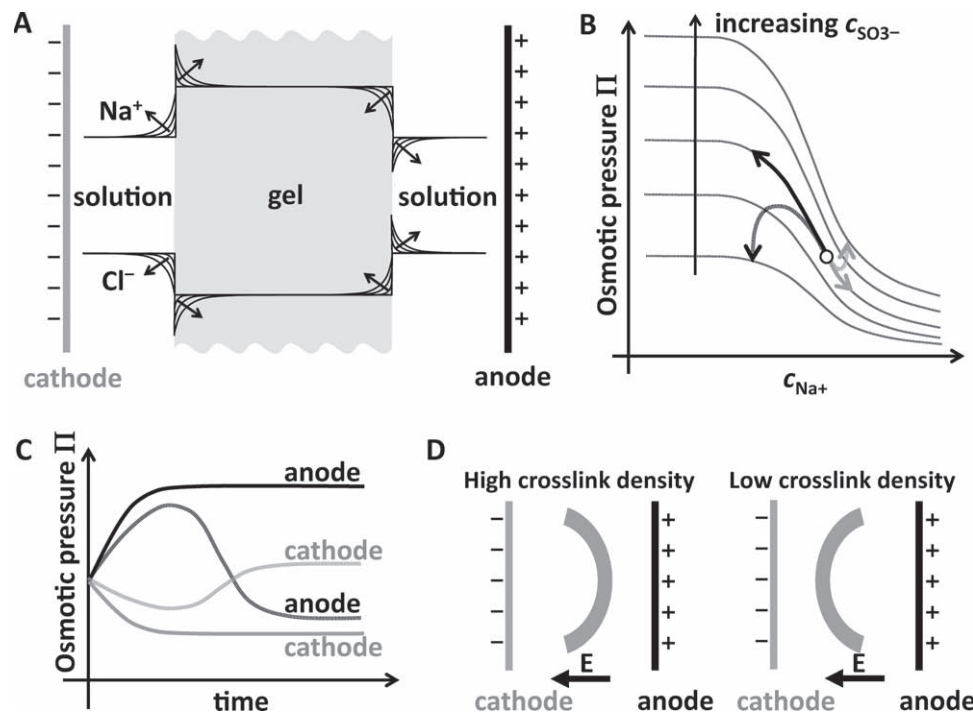
Enormous strides have been made in developing synthetic matrices with instructive cues mimicking the chemical aspects of the ECM to support in vitro cell culture. An important subset of these biomaterials are hydrogels, which possess several physical characteristics of the extracellular environment such as high water content, three-dimensional (3D) network structure, and facilitated mass transfer.[6,7] Most synthetic hydrogels can also be easily functionalized with bioactive motifs.[6,7] However, incorporation of dynamic biophysical cues like mechanical and electrical stimulation into these synthetic matrices still remains a challenge. Such biophysical cues have been reported to have many beneficial effects on different types of cells.[8–12] Current strategies for incorporating biophysical cues within in vitro systems rely on integrating biomaterials that provide structural support to the cells with bioreactors that provide biophysical cues.[13] Most available bioreactors provide either dynamic mechanical or electrical cues; however no approaches have been developed so far that can provide both cues simultaneously. It would therefore be desirable to develop multifunctional, synthetic matrices that can simultaneously provide structural support as well as chemical, electrical, and mechanical cues to the embedded cells in a 3D environment.[14]

Here we report the development of multifunctional, monolithic, hydrogel-based matrices that can simultaneously provide structural support and dynamic electrical and mechanical cues to the embedded cells. These matrices have the unique ability to undergo reversible, anisotropic bending dynamics in an electric field, akin to stretching-flexing behavior observed in various tissues such as skeletal muscles and cartilage. Moreover, the bending direction and magnitude can be tuned by varying the crosslink density. The conceptual design of these bidirectional hydrogels is motivated by theoretical modeling of the osmotic pressure at the anode and cathode side gel-solution interfaces. Our initial cell studies indicate that the matrices support cell viability, proliferation, and promote stem cell differentiation, as exemplified by chondrogenic differentiation of human mesenchymal stem cells (hMSCs).

H. L. Lim, J. C. Chuang, T. Tran, A. Aung, Prof. S. Varghese
Department of Bioengineering
University of California
San Diego, 9500 Gilman Drive, MC-0442, La Jolla, CA 92093, USA
E-mail: svarghese@ucsd.edu
Prof. G. Arya
Department of Nanoengineering
University of California
San Diego, 9500 Gilman Drive, MC-0448, La Jolla, CA 92093, USA
E-mail: garya@ucsd.edu

**ADVANCED
FUNCTIONAL
MATERIALS**

www.afm-journal.de

**Materials
Views**

www.MaterialsViews.com

Figure 1. Theoretical concept behind unidirectional and bidirectional bending hydrogels. (A) Expected accumulation of Na^+ and depletion of Cl^- ions at the cathode-side hydrogel boundary and depletion of Na^+ and accumulation of Cl^- ions at the anode-side hydrogel boundary with time. (B) Variation of osmotic pressure with solution Na^+ concentration for different concentrations of anionic groups (SO_3^-) within the gel. Solid arrows indicate the anticipated (from Doi theory) monotonic swelling and shrinkage of a high crosslink density hydrogel at the anode (black) and cathode (gray) sides, respectively. Dashed arrows indicate the non-monotonic swelling behavior (from modification of Doi theory) expected from a low crosslink density hydrogel as a result of swelling and shrinkage of the gel causing large changes in the concentration of anionic groups within the gel. (C) Time evolution of the osmotic pressure of a high and low crosslink hydrogels at the anode and cathode sides. Solid and dashed lines correspond to trajectories for high and low crosslink density hydrogels, respectively. (D) Steady-state bent conformation of high and low-crosslink hydrogels predicted by our modified theory.

2. Results

We first introduce the theoretical concept explaining how the crosslink density of polyelectrolyte hydrogels could be used to tune their extent and direction of bending within an electric field. We then describe the synthesis of anionic hydrogels and demonstrate their crosslink density dependent bidirectional bending behavior in an electric field. Finally, we describe proof-of-concept studies demonstrating the ability of these matrices to promote survival, proliferation, and differentiation of stem cells.

2.1. Theoretical Basis for Bidirectional Bending Hydrogels

It is well known that an elongated strip of an anionic hydrogel bends towards the cathode in an electric field.[15,16] Doi and coworkers have provided a comprehensive theory to explain this behavior.[17] We have extended this theory in conceptual terms by relaxing one of its assumptions that the concentration of gel anionic groups remains constant during the bending process, which leads us to a new scenario that the same anionic hydrogel can be made to bend in two different directions by changing its crosslink density. The details of the original Doi theory are provided in the Experimental section. Below we only discuss its salient points and our modification that led us to the design of bidirectional hydrogels.

Consider an anionic hydrogel poly (2-acryloylamido-2-methyl propane sulfonic acid) (PAMPS) containing SO_3^- within the electrolyte solution NaCl (**Figure 1**), which has been extensively studied as an electric field responsive hydrogel.[18] When an electric field is applied across the hydrogel, the Na^+ and Cl^- ions travel towards the cathode and anode, respectively. Under conditions of Donnan equilibrium, electroneutrality, and dissociation equilibria, the Doi theory shows that with time the interfacial concentration of Na^+ will increase and decrease at the cathode and anode sides, respectively (Figure 1A). At the same time, the interfacial concentration of Cl^- will decrease and increase at the cathode and anode sides, respectively (Figure 1A). The theory also shows that for hydrogels with a fixed concentration of anionic groups (c_{SO3^-}) that are fully dissociated, the osmotic pressure (Π) within the hydrogel decreases monotonically with increasing Na^+ concentration (c_{Na^+}) on the solution side, and that each Π–c_{Na} plot (at fixed c_{SO3^-}) shifts upward with increasing c_{SO3^-} (Figure 1B). This implies that Π will increase at the anode side (due to decreasing c_{Na^+}) and decrease at the cathode side (due to increasing c_{Na^+}). The solid black and gray arrows in Figure 1B schematically depict one such trajectory of Π vs. c_{Na^+} at the two hydrogel interfaces, and the solid black and gray lines in Figure 1C show the corresponding Π vs. time behavior. Thus, the model explains how anionic hydrogels swell at the anode side and shrink at the cathode side causing it to bend towards the cathode (Figure 1D left).

However, what has not been conceived so far is that an anionic hydrogel could be designed to swell on the cathode side and shrink at the anode side such that it bends towards the anode, exactly opposite to the behavior described above. Indeed such a hydrogel could be achieved if one realizes that the hydrogel swelling at the anode side is also accompanied by a decrease in the effective concentration of the anionic groups ($c_{SO_3^-}$). Similarly, as the hydrogel shrinks at the cathode side, the effective concentration of the anionic groups increases. This implies that the osmotic pressure trajectory at the anode side does not follow a single Π–c_{Na^+} curve but instead hops downwards to lower Π–c_{Na^+} curves corresponding to smaller $c_{SO_3^-}$ while climbing up each Π–c_{Na^+} curve. Therefore, we envision that if the change in $c_{SO_3^-}$ is sufficiently large, the trajectory will exhibit a maximum in the Π–c_{Na^+} plot and then dip downwards, as indicated by the black dashed arrow in Figure 1B and by the black dashed line in Figure 1C. At the cathode side, the osmotic pressure trajectory will hop to higher Π–c_{Na^+} curves due to the increase in $c_{SO_3^-}$ while climbing down each Π–c_{Na^+} curve, allowing for the possibility of a reversal in the direction of Π, as indicated by the gray dashed arrow in Figure 1B and gray dashed line in Figure 1C. Depending on the conditions, the final location of the osmotic pressure at the anode side could end up lower than that at the cathode (Figure 1B and Figure 1C), causing the gel to eventually bend towards the anode after transiently bending towards the cathode (Figure 1D right). The above trends, shown only schematically here, are described in a more quantitative manner in the Experimental section and Figure S1 of the Supporting Information.

The above analyses show that a hydrogel could conceivably change its bending direction. But, what kind of hydrogel would exhibit such a behavior? We propose that a sufficiently low crosslink density hydrogel could behave in the manner described above. Such gels are highly elastic and have the capacity to substantially swell at the anode and shrink at the cathode, causing large changes in the anionic group density that could lead to the reversal in osmotic pressure trajectories. We expect these hydrogels to initially bend towards the cathode, then straighten out, and eventually bend towards the anode (Figure 1D right). On the other hand, a highly crosslinked hydrogel that is relatively stiffer possesses little capacity to further swell or shrink in an electric field. The osmotic pressure of such a hydrogel would therefore be expected to exhibit the conventional monotonically increasing and decreasing osmotic pressure trajectory at the anode and cathode respectively, making the gel bend towards the cathode (Figure 1D left).
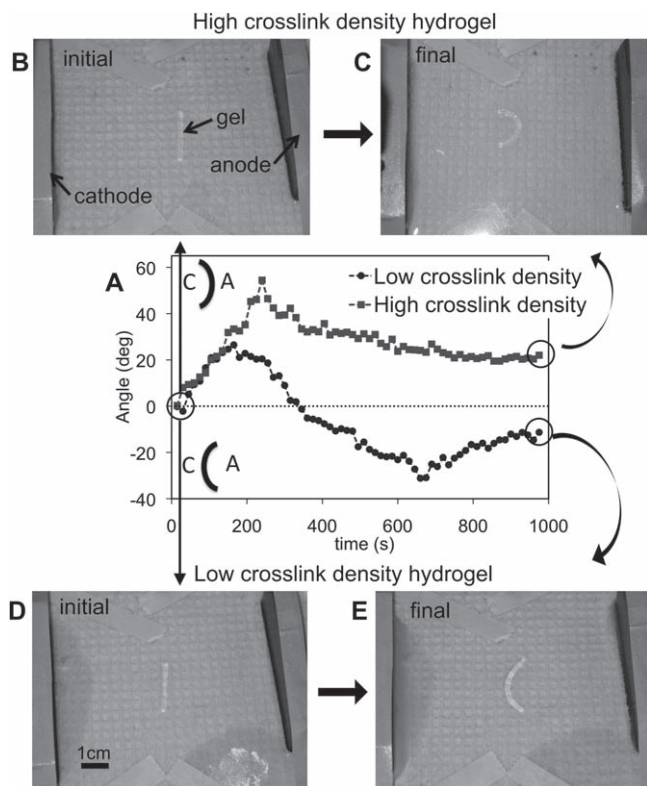
Although the above description utilizes PAMPS hydrogels in NaCl electrolyte as a model system to illustrate the main concept, in general, any anionic hydrogel in a suitable electrolyte should exhibit the crosslink density dependent reversal in bending discussed above.

2.2. Hydrogel Design and Bending Measurements

Guided by the above theoretical predictions, we synthesized PAMPS anionic hydrogels of two different crosslink densities: low (~20 µmol/cm³) and high (~200 µmol/cm³) to examine if the two anionic hydrogels could bend in opposite directions. Equilibrium swollen hydrogel strips of dimension 2 mm × 2 mm × 20 mm were placed within a custom designed direct current (DC) electrochemical cell such that the longer dimension was parallel to the electrode surfaces (**Figure 2**). We used
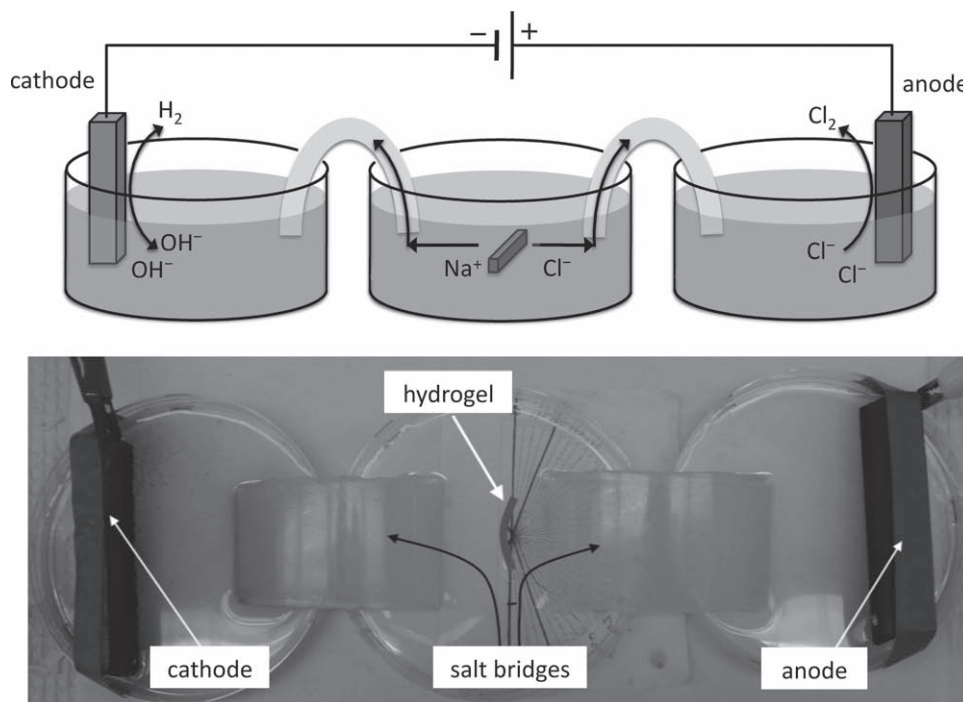
Figure 2. Setup of a Daniell electrochemical cell used for subjecting hydrogels to an electric field, consisting of separate cathode, anode, and hydrogel chambers separated by agarose salt bridges.

ADVANCED
FUNCTIONAL
MATERIALS

www.afm-journal.de

FULL PAPER

Materials
Views

www.MaterialsViews.com

Figure 3. (A) Time evolution of the bending angle for low crosslink density (circles) and high crosslink density (squares) hydrogels. Schematic of the bending configuration for positive and negative angles is given, where A and C stand for anode and cathode, respectively. The initial and final, steady-state configuration of the high crosslink density hydrogel (B,C) and low crosslink density hydrogels (D,E) are also shown.

phosphate buffered saline solution (PBS) as the electrolyte to be consistent with cell culture requirements in our subsequent cell studies. The voltage potential gradient across the gel was maintained at ~0.5 V/mm. See Experimental section for hydrogel synthesis and electrochemical setup.

We next tested the effect of a DC electric field on the two PAMPS hydrogels with different crosslink densities. **Figure 3**A shows the time evolution of the bending angle of the hydrogels in the electric field starting from a straight configuration (Figure 3B,D). Note that positive and negative angles represent bending towards the cathode and anode, respectively. The high crosslink density PAMPS hydrogel quickly reached a maximum bending angle of +50° in 4 min, and then slowly decreased to a steady state bending angle of +20° after 12 min. Figure 3C shows this final steady state configuration. To confirm that the above bent configuration represents the steady state and not a transient state, we manually rotated the hydrogel by 180° in the horizontal direction. The hydrogel indeed reverted to its original bending direction, indicating that it had acquired the most energetically favorable state. Furthermore, the hydrogels maintained this bent configuration for over an hour (maximum experimental time) in the electric field.

The low crosslink density PAMPS hydrogel, on the other hand, exhibited a very different behavior (Figure 3A). The hydrogel first bent towards the cathode similar to the highly crosslinked

hydrogel till it reached a maximum bending angle of +25°. This initial bending happened very fast (<2 min). The bending angle then started decreasing. However, in contrast to the high crosslink density hydrogel, the bending angle kept on decreasing until the gel started bending towards the anode. The hydrogel reached a maximum angle of −30° (11 min) before decreasing to a steady-state bending angle of −12° (15 min) (Figure 3E). As before, we confirmed the steady-state nature of this final bent configuration by flipping the hydrogel in the opposite direction and also leaving it in the electric field for over an hour. Hence, the same hydrogel could be designed to bend towards the anode or cathode by varying its crosslink density, as predicted theoretically.

It is also instructive to examine the swelling ratio of the two types of hydrogels, before the introduction of the electric field (equilibrium swelling) and in the final bent configuration in the presence of the electric field. As expected, the low crosslink density hydrogels (11.3 g/g) exhibited a larger equilibrium swelling ratio compared to the high crosslink density hydrogels (6.91 g/g). Interestingly, the low crosslink density hydrogel swelled significantly more in the presence of the electric field, achieving a swelling ratio as large 25 g/g, compared to its high crosslink density counterpart that only swelled slightly (8.6 g/g). Indeed, it is this capacity of the low crosslink density hydrogels to swell significantly more in electric field that causes them to reverse their bending direction, as suggested by our modified theory.

To investigate if the crosslink density dependent differential bending of hydrogels is functional group and hydrogel precursor dependent, we have repeated the above set of experiments for acrylic acid (AA) hydrogels and acryloyl 6-aminocaproic acid hydrogels (A6ACA), both carrying carboxyl functional groups, and poly(ethylene glycol)-chondroitin sulfate (PEG/CS) hydrogels, carrying sulfate functional groups. We observed a similar crosslink density dependent bending behavior, indicating that the observed bidirectional-bending phenomenon is primarily dependent on the crosslink density, though the quantitative values of the bending angle and the swelling ratio vary from hydrogel to hydrogel (data not shown).

We have also demonstrated that the above electric field responsive hydrogels can exhibit continuous flexing and straightening cycles in response to an electric field that switches on and off periodically. This could be important from the point of view of cell culture where cells may require dynamic biophysical cues. To this end, we subjected the high-crosslink density PAMPS hydrogels to such a periodic applied electric field with a frequency of 10 min, where the electric field is on for 1 min and off for 9 min. **Figure 4** shows the response of the high crosslink density PAMPS hydrogel in terms of the mechanical strain (deduced from volume measurements). The additional swelling attained with 1-min imposition of the electric field took almost 9 min to relax to its original volume. The hydrogels exhibited a reversible flexing-straightening dynamics over two hours (12 cycles; maximum experimental time). Note that in order to obtain good signal-to-noise ratio, we employed cyclic electric fields with periods on the order of minutes. However, we expect that a range of bending amplitudes and frequencies and strains could be achieved through manipulation of the field strength and frequency, hydrogel aspect ratio, and material properties such as crosslink density and number of anionic groups.

www.MaterialsViews.com

ADVANCED
FUNCTIONAL
MATERIALS
www.afm-journal.de

FULL PAPER
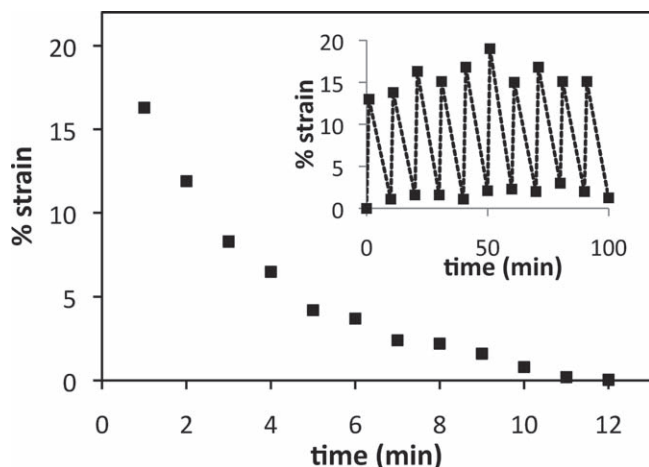
Figure 4. Percentage strain relaxation of a bent PAMPS hydrogel strip in the absence of electric field, where the bent strip was produced by switching on the electric field at time zero and switching it off at 1 minute. Inset shows the measured strain in the hydrogel strip subjected to cyclic on-off electric field (1 min on and 9 min off). Only the lowest and highest strain values are plotted.

2.3. Cell Culture Studies

We used PAMPS hydrogels for characterizing electric-field mediated bending of anionic hydrogels because (i) AMPS monomers are readily available off-the-shelf and (ii) the hydrogel crosslink density could be easily controlled (by varying the bis-acrylamide crosslinker content), which allowed us synthesize a large number of hydrogel strips required to generate the results described above. However, AMPS monomers do not support encapsulation of cells; therefore we use PEG/CS hydrogels to evaluate the potential of electromechanical matrices for supporting cells. We find that the PEG/CS hydrogels exhibit similar bending as PAMPS hydrogels in the presence of an electric field. The time evolution of the bending angle of PEG/CS hydrogels and their percentage strain relaxation in response to electric fields is shown in Figure S2. Moreover, we have previously shown that PEG/CS hydrogels without electric field can support MSCs growth and their chondrogenic differentiation.[19]

We investigated the potential benefit of electric field responsive hydrogels on cell viability by subjecting hMSCs-laden PEG/CS hydrogel to an electric field. The hMSCs (p7043L, Tulane University) were encapsulated within PEG/CS hydrogels using photopolymerization (see Experimental section). These hMSC-laden hydrogels (2 mm × 2 mm × 20 mm) were then subjected to an electric field as described before. Similar to the acellular PEG/CS hydrogels, the cell-laden PEG/CS hydrogels also exhibited electric field induced bending (Figure S3). As before, a potential gradient of 0.5V/mm across the hydrogel was used to yield a potential gradient of ~5mV across a single cell, similar to reported values.[20] The volume fraction of

cells within the hydrogels was sufficiently low (~0.01) such that it did not affect any material properties of the hydrogel and its electric field response.

We conducted two types of experiments: (i) *continuous*, where we subjected the hydrogels to an electric field for 30 min every day and the gels remained bent throughout; and (ii) *dynamic*, where we subjected the hydrogels to an electric field that switches on and off in a cyclic manner for 30 min every day (1 min on, 4 min off) and the hydrogels stretched and flexed periodically during this time. The viability of the embedded cells over seven days of exposure to the electric field was analyzed by live/dead assay (see Experimental section). **Figure 5**A and Figure S4A show that almost all cells subjected to continuous and dynamic electric fields remained viable, similar to the control cell-laden PEG/CS hydrogels that were not exposed to an electric field. The effect of electro-mechanical matrices on cell viability was also evaluated for other cells types such as chondrocytes and muscle progenitor cells (C2C12 cells); they all exhibited similar cell viability (>90%).

In addition to cell viability, we also evaluated the effect of electro-mechanical matrices on cell proliferation. Ki67 staining for hMSCs-laden hydrogels after 5 days of exposure to continuous electric field (exposed to the electric field for 30 min continuously per day) suggested that the electro-mechanical matrices promote cell proliferation (Figure S4B,C). We also analyzed the long-term effect of these matrices on cell cultures, where the cell-laden hydrogels were subjected to a continuous (exposed to electric field for 30 min continuously per day) electric field for 21 days. As analyzed by the TUNEL staining, the cells again showed good cell viability suggesting no detrimental effect from the electric field (Figure S4D). A time-dependent increase in hMSC proliferation was observed over 21 days of culture in continuous electric field, which was found to be better than their corresponding control cultures which were not exposed to electric field (Figure 5B).

We have further evaluated the ability of the above matrices to assist chondrogenic differentiation of hMSCs (**Figure 6**). After 21 days of culture in chondrogenic conditions, the hMSCs in hydrogels exposed to electric field in the continuous mode exhibited higher chondrogenic differentiation compared to those grown in similar conditions without the electric field (control). This trend is consistent between cultures containing
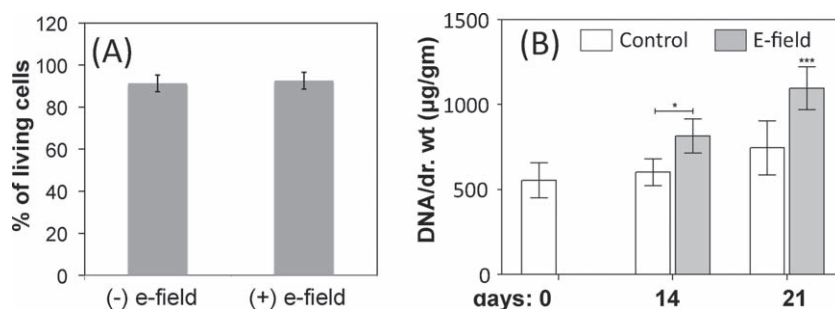
Figure 5. Effect of electro-mechanical matrices (PEG/CS hydrogels) on encapsulated cells. (A) Percentage viable hMSC cells after five days of culture in the presence (averaged over continuous and dynamic experiments) and absence of electric field. (B) DNA measurement of hMSCs as a function of culture time in electric field (continuous mode) and without electric field (control).

ADVANCED
FUNCTIONAL
MATERIALS
www.afm-journal.de

Materials
Views
www.MaterialsViews.com
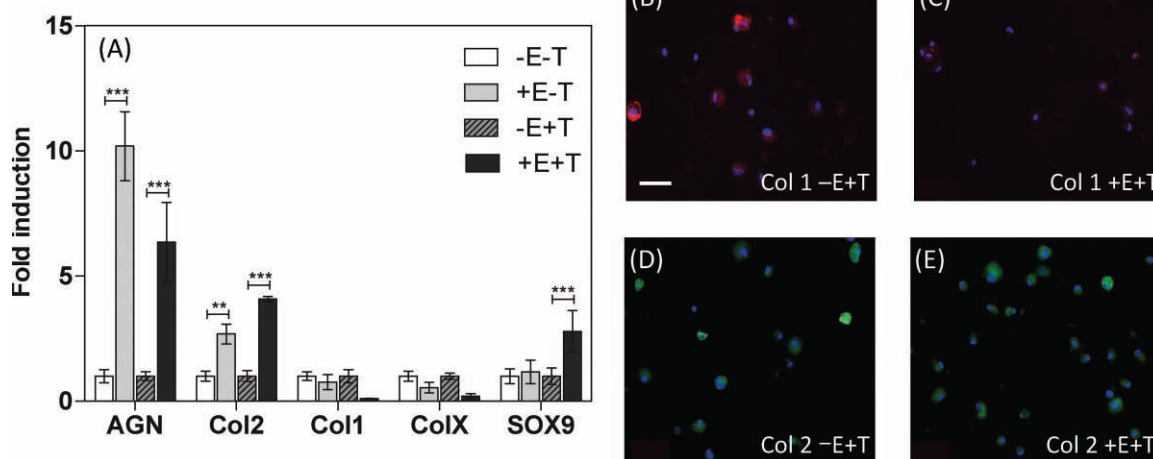
Figure 6. (A) Real time PCR analysis of hMSCs in various culture conditions for 21 days in continuous electric field mode (30 min per day). AGN: aggrecan; Col 2: type II collagen; Col 1: type 1 collagen; Col X: type X collagen; and Sox9. In culture conditions labeled –E–T, +E–T, –E +T, and +E +T, +E and –E represents presence and absence of electric field, respectively, and +T and –T represent presence and absence of TGF-β1, respectively. Images of collagen type I staining for –E+T (B) and +E+T (C) and collagen type II staining for –E+T (D) and +E+T (E) are also shown. The scale bar represents 50 μm for all images.

or absent in TGF-β1, as noted from the gene expression profile (Figure 6A). Specifically, hMSCs exposed to electric field expressed higher levels of aggrecan and collagen type II expression both in the presence and absence of TGF-β1. In contrast, hMSCs exposed to electric field exhibited lower levels of collagen types I and X in the presence of TGF-β1 and no changes in the absence of TGF-β1 (Figure 6A). The production and accumulation of matrix components were detected by immunoflourescent staining. The differentiated hMSCs in both the cultures stained positive for collagen types 1 and 2, but exhibited notable differences in their intensity (Figure 6B–E). Note that due to the presence of CS moieties in the hydrogel, the entire section stained positive for Safranin-O.

3. Discussion

Most electric field responsive hydrogels reported so far only bend in a single direction in the presence of an electric field. We introduce here anionic hydrogels that can be tuned to bend in both directions in an electric field by manipulating a single material parameter, the crosslink density. Interestingly, this concept emerged from a modification of the theory developed by Doi and coworkers to explain anionic hydrogel bending towards the cathode. By accounting for changes in the concentration of anionic groups within the hydrogel as it swells and shrinks at the anode and cathode sides, respectively, we show that hydrogels could be made to reverse their bending direction by lowering their crosslink density. Indeed, this concept is not limited to anionic gels, and we expect that cationic gels that originally bend towards the anode could also be made to reverse their bending direction by exploiting this phenomenon. To our knowledge, there exist two studies that have reported hydrogels that initially bend towards the cathode and then towards the anode in the presence of an electric field, though the origin of such a behavior was not established.[20,21] In another study,

Shiga et al.[22] demonstrated that poly(vinyl alcohol)-poly(sodium acrylate) can change their bending direction, depending upon solution conditions (neutral or basic).

One of the main motivations for developing these hydrogels was that it would allow us to combine two physiologically important biophysical cues—mechanical strain and electric potential—into one synthetic matrix that has already been proven to provide structural support and chemical cues to cells. Indeed, electrical and mechanical cues have been shown to play a profound role in embryogenesis, differentiation, protein synthesis, and tissue repair.[4,5,8,11,23–29] To facilitate cell studies, we have built a customized electrochemical cell that involves compartmentalization of cell-laden hydrogels and electrodes to prevent electrolyte waste generated at the electrodes from contaminating the cells. Such a setup allows us to apply electric fields for more than an hour at a stretch, which could be prolonged further by periodically replacing salt bridges and electrolyte waste reservoirs.

Using such a setup, we have demonstrated the viability of various types of cells, both differentiated and stem cells, encapsulated within PEG/CS hydrogels when exposed to continuous and dynamic modes of electric field exposure. The hydrogels exposed to the electric field also promoted stem cell proliferation in accordance with previous studies which demonstrated upregulation of DNA synthesis in cartilage cells by oscillating electric fields after short stimulation.[30] Additionally, the electric field stimulated PEG/CS hydrogels exhibited enhanced chondrogenic differentiation compared to those without electric field exposure. This enhancement in proliferation and differentiation could be attributed to either the electrical excitation or the mechanical stimuli or both. However, dissecting the contribution from each cue was not attempted here, as our primary goal was to develop and validate the potential of electric field mediated, multi-functional matrices for 3D stem cell culture. Detailed studies on decoupling contributions of mechanical and electrical cues to stem cells, their dependence on parameters

www.MaterialsViews.com

ADVANCED
FUNCTIONAL
MATERIALS
www.afm-journal.de

FULL PAPER

such as frequency and length of stimulation, and effects of the bending planes (compressive, neutral, or tensile side) with hydrogel strips are currently underway in our laboratory. To our knowledge, our study represents the first demonstration of cell culture in an electric field-responsive hydrogel, which can provide both mechanical and electrical cues simultaneously to the cells.

4. Conclusions

We have developed dynamic, multifunctional matrices whose direction of bending can be controlled through the crosslink density. Our initial studies demonstrate that these matrices functioning under dynamic and continuous electric fields could support long term cell survival, proliferation and chondrogenic differentiation of hMSCs. Such multi-functional matrices not only provide a synthetic platform to simultaneously provide multiple biophysical cues to cells, but also can be used to dissect the effect of individual biophysical cues on various cellular behaviors from each other. Additionally, one could foresee that the differential swelling of hydrogels in an electric field could be used to deliver drugs to tissues in a direction dependent manner. Finally, such electro-mechanical hydrogels could be useful for high-throughput screening of mechano-sensory cells for drug discovery.

5. Experimental Section

Doi theory for electric field mediated bending of anionic hydrogels: We derive the expression for osmotic pressure within an anionic hydrogel possessing dissociable anionic groups (SO_3^-) as a function of the electrolyte NaCl concentration, following the theory introduced by Doi and coworkers.[17] Consider the hydrogel placed in an electric field. The gel swells in the water due to the development of an osmotic pressure, $\Delta\Pi$, which is given by

$$\Delta\Pi = RT \sum_i \left(c_{i,g} - c_{i,s} \right) \tag{1}$$

where R is the gas constant, T is the temperature, and $c_{i,g}$ and $c_{i,s}$ are the concentration of ionic species inside the hydrogel and solution, respectively, and i represents the four ionic species present in the system: Na^+, Cl^-, H^+, and OH^-. The well-known Donnan equilibrium condition provides a relationship between the ion concentrations on either side of the hydrogel boundary

$$\frac{c_{Na^+,g}}{c_{Na^+,s}} = \frac{c_{H^+,g}}{c_{H^+,s}} = \frac{c_{Cl^-,s}}{c_{Cl^-,g}}$$
$$= \frac{c_{OH^-,s}}{c_{OH^+,g}} = \exp\left(-\Delta\psi\right) \equiv P \tag{2}$$

where $\Delta\psi$ is the normalized electrostatic potential difference across the hydrogel-solution boundary and P represents the partition coefficient. Next, we invoke the condition of electroneutrality in the hydrogel and solution phases

$$c_{Na^+,s} + c_{H^+,s} = c_{Cl^-,s} + c_{OH^-,s} \tag{3}$$

$$c_{Na^+,g} + c_{H^+,g} = c_{Cl^-,g} + c_{OH^-,g} + c_{SO_3^-,g} \tag{4}$$

The concentrations of H^+ and OH^- are dictated by the dissociation constant of water, K_w

$$c_{H^+,g}c_{OH^-,g} = c_{H^+,s}c_{OH^-,s} = K_w \tag{5}$$

Given the large dissociation constant of the SO_3H, we can assume that these groups are fully dissociated and hence the concentration of ionized SO_3^- groups is fixed.

Using Equation (1–5), one can easily solve for the concentration of H^+ ions in the solution phase, the partition coefficient, the osmotic pressure, and the concentration of Na^+ and Cl^- ions in the hydrogel phase

$$c_{H^+,s} = \frac{1}{2}\left[c_{Cl^+,s} - c_{Na^+,s} + \sqrt{(c_{Na^+,s} - c_{Cl^-,s})^2 + 4K_w} \right] \tag{6}$$

$$P = \frac{c_{SO_3^-,s} + \sqrt{c_{SO_3^-,s} + 4(c_{Na^+,s} + c_{H^+,s})}}{2(c_{Na^+,s} + c_{H^+,s})} \tag{7}$$

$$\Pi/RT = \sqrt{(c_{SO_3^-,s})^2 + 4(c_{Na^+,s} + c_{H^+,s})^2}$$
$$- 2(c_{Na^+,s} + c_{H^+,s}) \tag{8}$$

$$c_{Na^+,g} = Pc_{Na^+,s}$$
$$c_{Cl^-,g} = c_{Na^+,s}/P \tag{9}$$

where $P > 1$, as the hydrogel is anionic and the concentration of Na^+ will be higher inside the hydrogel than in the solution.

We next examine fluxes of Na^+ and Cl^- inside and outside the hydrogel to evaluate changes in their concentration at the hydrogel/solution interface. We invoke the electroneutral condition on the solution side of the hydrogel boundary

$$c_{Na^+,s} = c_{Cl^-,s} \equiv c_0 \tag{10}$$

If we assume a constant *total* ionic flux J at the beginning, then the initial velocity of the ions in the solution and the hydrogel are given by (using Equation 9 and 10):

$$V_s = J/(c_{Na^+,s} + c_{Cl^-,s}) = J/(2c_0)$$
$$V_g = J/(c_{Na^+,g} + c_{Cl^-,g}) = J/(c_0 P + c_0/P) \tag{11}$$

Hence, the individual flux of Na^+ and Cl^- ions in the solution and hydrogel $J_{Na^+,s}, J_{Cl^-,s}, J_{Na^+,g}, \text{and} J_{Cl^-,g}$ are given by

$$J_{Na^+,s} = c_{Na^+,s}J/(c_{Na^+,s} + c_{Cl^-,s}) \equiv J/2$$
$$J_{Na^+,g} = c_{Na^+,g}J/(c_{Na^+,g} + c_{Cl^-,g}) \equiv JP^2/(1 + P^2)$$
$$J_{Cl^-,s} = c_{Cl^-,s}J/(c_{Na^+,s} + c_{Cl^-,s}) \equiv J/2$$
$$J_{Cl^-,g} = c_{Cl^-,g}J/(c_{Na^+,g} + c_{Cl^-,g}) \equiv J/(1 + P^2) \tag{12}$$

implying that the ratio of the fluxes is given by

$$\frac{J_{Na^+,g}}{J_{Na^+,s}} = \frac{c_{Na^+,g}}{c_{Na^+,s}}\left(\frac{c_{Na^+,s} + c_{Cl^-,s}}{c_{Na,g} + c_{Cl,g}}\right) \equiv \frac{2P^2}{(1+P^2)} > 1$$
$$\frac{J_{Cl^-,g}}{J_{Cl^-,s}} = \frac{c_{Cl^-,g}}{c_{Cl^-,s}}\left(\frac{c_{Na^+,s} + c_{Cl^-,s}}{c_{Na^+,g} + c_{Cl^-,g}}\right) \equiv \frac{2}{(1+P^2)} < 1 \tag{13}$$

Equation 13 implies that the flux of Na^+ is always greater in the hydrogel compared to the solution due to its greater concentration there, while the opposite is true for Cl^-. Therefore, at the *anode* side, the incoming solution Na^+ flux is lower than the outgoing hydrogel Na^+ flux, causing Na^+ to get depleted at the anodic gel interface (Figure 1A top). In contrast, at the *cathode* side, the incoming gel Na^+ flux is higher than the outgoing solution Na^+ flux causing accumulation of Na^+ at the hydrogel

interface (Figure 1A top). Using the same argument, one can show that Cl^- ions get accumulated at the anode side hydrogel-interface and get depleted at the interface on the cathode side (Figure 1A bottom).

From the osmotic pressure relationship (Equation 8), it is noted that Π is a function of only $c_{Na+,s}$, $c_{H+,s}$, and c_{SO3^-}. Specifically, when $c_{H+,s} \ll c_{Na+,s}$ as is the case for the PAMPS hydrogels examined here, Π is a monotonically decreasing function of $c_{Na+,s}$ given by

$$\Pi/RT = 2c_{Na^+,s}\left(\sqrt{1 + (c_{SO_3^-,g}/2c_{Na^+,s})^2} - 1\right) \tag{14}$$

This function is schematically plotted in Figure 1B for several anionic group concentrations c_{SO3^-}. This implies Π should rise with time on the anode side of the hydrogel, where the Na^+ concentration decreases with time, while Π should decrease on the cathode side, where the Na^+ concentration increases with time. In other words, Π increases along the solid black arrow at the anode side and Π should decrease along the solid gray arrow (Figure 1B). Thus, the hydrogel should swell on the anode side and shrink at the cathode side with time, causing it to bend towards the cathode side, as shown in Figure 1D (left), as previously observed by several studies.

Numerical analyses of modified Doi theory: We have numerically investigated the modified Doi theory to examine if it can reproduce the dynamics of our low crosslink density hydrogels, which bend towards the anode when subjected to an electric field in a PBS buffer, opposite to the behavior predicted by Doi theory. To this end, we input into the model the relevant parameters associated with the hydrogel and buffer.

The PAMPS hydrogel employed in the study contains fully dissociated SO_3^- anionic groups at an approximate concentration of $c_{SO3^-} = 0.2$ M. The PBS buffer is essentially a 1:1 electrolyte containing various anionic and cationic species of which Na^+ and Cl^- are the primary ionic species. The net concentration of monovalent cations and anions is close to the physiological value of $c_0 \approx 0.15$ M. We also assume that the Na^+ concentration in the solution at the anode-side interface of the hydrogel decreases from $c_{Na+,s} = 0.15$ M to 0.01 M in a time-dependent power-law manner. The Na^+ concentration in the solution at the cathode-side interface also rises in a power-law manner from $c_{Na+,s} = 0.15$ M to 0.2 M (Figure S1A). We also assume that due to the swelling and shrinkage of the hydrogel at the anode and cathode sides, respectively, the concentration of anionic group changes from $c_{SO3^-} = 0.2$ M to 0.1 M and 0.3 M in a power-law manner (Figure S1B). As expected, the characteristic timescale for gel swelling and shrinkage is taken to be slower than the time scale associated with the rise and dip in Na^+ concentration at the hydrogel interface. Figure S1C and Figure S1D show the $\Pi-c_{Na+}$ and $\Pi-t$ curves obtained using the above parameters. Clearly, the modified model explains the initial bending of the PAMPS hydrogel towards the cathode, the reversal in its bending direction, and the final steady state configuration of the hydrogel bent towards the anode.

Synthesis and characterization of hydrogels: The hydrogels were synthesized using poly (ethylene glycol) diacrylate (PEGDA) having a molecular weight M_n of 6000 g/mol . Low crosslink density PAMPS hydrogels were prepared by dissolving 4% (w/v) PEGDA in 1M solution of AMPS (vendor) in de-ionized water. To this solution, 0.1% Irgacure D2959 (Cibca Specialty Chemicals, Tarytown, NY) was added and the homogenously mixed solution was polymerized using a long wavelength 365 nm light at 4.5 mW/cm² (VWR) for 5 min.[19] We used 30% (w/v) PEGDA to create PAMPS hydrogels with higher crosslink density. The gels were swelled in PBS until they reached equilibrium swelling. Uniform strips of gel measuring 20 mm × 2 mm × 2 mm were cut out from the PBS-equilibrated hydrogels for electric field experiments. The PEG/CS hydrogels were synthesized using 5% (w/v) PEGDA having a molecular weight M_n of 6000 g/mol and 10% (w/v) methacrylated CS, as described elsewhere.[19] The crosslink density of the hydrogels was calculated from the experimentally obtained modulus using $\sigma = \nu_e kT(\alpha - 1/\alpha^2)$, where σ is the stress, ν_e is the number of elastically active chains, k is the Boltzmann constant, T is the absolute temperature, and α is the strain. The weights of the gels were obtained before and after electric field exposure and the swelling ratio was calculated as

the weight of the solvent uptake per unit mass of the dried polymer. For cell encapsulation, the cells (hMSCs, chondrocytes, and C2C12) were suspended within the precursor solution (12–15 million cells/ml), transferred into a sterile glass mold, and photopolymerized (see above) for 5 min to yield cell-laden hydrogels.

Electrochemical cell setup: The experimental setup involves an optimized Daniell cell to isolate the electrolytic waste from the central compartment carrying the hydrogel using agarose salt bridges (2%) (Figure 2). The electric current manifested through ion migration across the two electrodes maintained electroneutrality. The electrolytic waste comprises of hydroxide ions that are liberated at the cathode and chlorine gas liberated at the anode. The hydroxide ions were tracked using phenolphthalein that produces a distinct pink color when the hydroxide ions migrates into the agarose, allowing us to detect any pH changes taking place in the hydrogel carrying compartment. The graphite electrodes connected to the power supply and the input voltage were adjusted to generate a potential gradient of 0.5 V/mm within the hydrogel and thereafter kept fixed. A digital multimeter was used to measure the electric potential differences across the gels and a protractor placed beneath the hydrogel compartment was used for bending angle measurements.

Cell culture: hMSCs (p7043L, Tulane University, New Orleans, LA) were expanded in growth medium (alpha-MEM, 10% fetal bovine serum (FBS), 2 mM glutamine, and 50 units/mL penicillin/streptomycin). For all experiments described here, passage 4 hMSCs were employed. Primary bovine chondrocytes were isolated and expanded as described elsewhere.[31] C2C12 cells were purchased from ATCC and cultured in DMEM containing 10% FBS. The cell-laden hydrogels were cultured in high glucose DMEM containing 10% FBS.

Chondrogenic differentiation of hMSCs-laden hydrogels: The hMSC-laden hydrogels were cultured in chondrogenic medium (500 mL high glucose DMEM containing 100 nM dexamethasone, 50 μg/mL ascrobate-2-phosphate, 40 μg/mL proline, 100 μg/mL sodium pyruvate, 1% penicillin streptomycin, 6.25 ng/mL insulin, 6.25 mg transferiin, 6.25 ng/mL selenious acid, 1.25 mg/mL bovine serum albumin, and 5.35 mg/mL linoleic acid) with and without 10 ng/mL TGF-β1. During the electric field stimulation, we transferred the cell-laden hydrogels into DMEM containing 10% FBS and no TGF-β1.

Live/dead assay: Viability of cell laden hydrogels was determined by the Live/Dead Viability/Cytotoxicity Kit (Molecular Probes, Eugene, OR), which contains calcein-AM ("Live" dye) and ethidium homodimer-1 ("Dead" dye). The cell-laden hydrogels were washed with PBS and sectioned into thin slices. These slices were then incubated for 30 min in "Live/Dead" dye solution containing 0.5 μL of calcein-AM dye and 2 μL of ethidium homodimer-1 dye in 1 mL DMEM. The percentage of viable cells were determined by counting the live cells, which were stained with green dye, relative to all cells present averaged over six different fields per experiment and three different experiments.[19] We also evaluated the cell viability over long-term exposure to electric field by TUNEL staining. Cell-laden hydrogels exposed to 21 day (30 min per day) of electric field were cryo-sectioned and stained for apoptotic cells using TdT-mediated dUTP nick-end labeling (TUNEL) assay (Chemicon, CA).[19] Similarly, the Ki67 staining for cell proliferation was carried out using FITC-conjugated rabbit polyclonal antibody (Abcam). The stained sections were mounted with VectaShield-DAPI (Vector Laboratories, Burlingame, CA). All the images were taken using a Zeiss Observer A1 microscope equipped with an X-Cite 120 (EXFO) mercury lamp.

DNA content: The time dependent cell growth of hMSCs encapsulated within the hydrogel matrices was evaluated by DNA measurements. The lyophilized cell-laden hydrogels were crushed using pellet pestle mixer (Kimble/Kontes) and digested in papainase solution (construct/1 mL papainase solution; 125 μg/mL; Worthington Biomedical, Lakewood, NJ) for 18 hrs at 60 °C. The DNA content was determined using PicoGreen dsDNA quantification kit.

Gene expression analysis using real-time PCR: Total RNA was extracted from three cell-laden hydrogels with Trizol, and reverse-transcribed into cDNA using SuperScript First-Strand Synthesis System (Invitrogen). 1 μL aliquots of the resulting cDNA were amplified at the corresponding

www.MaterialsViews.com

ADVANCED
FUNCTIONAL
MATERIALS
www.afm-journal.de

FULL PAPER

annealing temperature for 35 cycles. The PCR primers are listed in Table S1. PCR products were separated by electrophoresis at 100V on a 2% agarose gel in Tris-acetate-EDTA buffer and visualized after ethidium bromide staining.

Immunoflourescent staining: For immunostaining, hMSC-laden PEGDA hydrogels (constructs) were fixed overnight in 4% paraformaldehyde (pH 7.4) at room temperature and transferred to 70% ethanol at 4 °C until processing. Cell-laden hydrogels were then embedded in OCT and cryosectioned into 30–50 μm sections. For immunostaining, sections were blocked in blocking buffer (3% BSA and 0.1% Triton-X 100 in 1X PBS) for 1 hour and incubated with Fitzgerald rabbit polyclonal antibodies against types I or II collagen (RDI) with 1:250 dilutions. Sections were then incubated with either FITC- or Texas red conjugated goat anti-rabbit secondary antibody, or Alexa Fluor 488 (all 1:300 dilutions) for 1 hour. Nuclei were counterstained with DAPI (Chemicon) mounting medium and stored in dark at −20 °C, and images were collected on a Zeiss fluorescent microscope, Axio Observer A1.

Supporting Information

Acknowledgements

[1] T. Rozario, D. W. Desimone, *Dev. Biol.* **2009**, *34*, 126.
[2] N. Gjorevski, C. M. Nelson, *Cytokine Growth Factor Rev.* **2009**, *20*, 459.
[3] D. E. Discher, D. J. Mooney, P. W. Zandstra, *Science* **2009**, *324*, 1673.
[4] M. Levin, *Semin. Cell. Dev. Biol.* **2009**, *20*, 543.
[5] F. Guilak, D. M. Cohen, B. T. Estes, J. M. Gimble, W. Liedtke, C. S. Chen, *Cell. Stem. Cell.* **2009**, *5*, 17.
[6] M. P. Lutolf, J. A. Hubbell, *Nat. Biotechnol.* **2005**, *23*, 47.
[7] S. Varghese, J. Elisseeff, *Adv. Polym. Sci.* **2006**, *203*, 95.
[8] M. Radisic, H. Park, H. Shing, T. Consi, F. J. Schoen, R. Langer, L. E. Freed, G. Vunjak-Novakovic, *Proc. Natl. Acad. Sci. USA* **2004**, *101*, 18129.
[9] W. L. Grayson, T. P. Martens, G. M. Eng, M. Radisic, G. Vunjak-Novakovic, *Semin. Cell. Dev. Biol.* **2009**, *20*, 665.
[10] H. Park, R. Bhalla, R. Saigal, M. Radisic, N. Watson, R. Langer, G. Vunjak-Novakovic, *J. Tissue Eng. Regen. Med.* **2008**, *2*, 279.
[11] E. Serena, E. Figallo, N. Tandon, C. Cannizzaro, S. Gerecht, N. Elvassore, G. Vunjak-Novakovic, *Exp. Cell. Res.* **2009**, *315*, 3611.
[12] G. H. Altman, R. L. Horan, I. Martin, J. Farhadi, P. R. Stark, V. Volloch, J. C. Richmond, G. Vunjak-Novakovic, D. L. Kaplan, *FASEB J.* **2002**, *16*, 270.
[13] J. A. Burdick, G. Vunjak-Novakovic, *Tissue Eng. Part A* **2009**, *15*, 205.
[14] P. Fratzl, F. G. Barth, *Nature* **2009**, *462*, 442.
[15] T. Shiga, *Neutron Spin Echo Spectroscopy Viscoelasticity Rheology* **1997**, *134*, 131.
[16] T. Tanaka, I. Nishio, S. T. Sun, S. Uenonishio, *Science* **1982**, *218*, 467.
[17] M. Doi, M. Matsumoto, Y. Hirose, *Macromolecules* **1992**, *25*, 5504.
[18] Y. Osada, H. Okuzaki, H. Hori, *Nature* **1992**, *355*, 242.
[19] S. Varghese, N. S. Hwang, A. C. Canver, P. Theprungsirikul, D. W. Lin, J. Elisseeff, *Matrix Biol.* **2008**, *27*, 12.
[20] W. M. Lai, D. D. Sun, G. A. Ateshian, X. E. Guo, V. C. Mow, *Biorheology* **2002**, *39*, 39.
[21] I. A. Rousseau, , *Mater. Res. Soc. Proc* **2002**, *698*, 1.
[22] T. Shiga, Y. Hirose, A. Okada, T. Kurauchi, *J. Appl. Poly. Sci.* **1993**, *47*, 113.
[23] T. Lecuit, P. F. Lenne, *Nat. Rev. Mol. Cell. Biol.* **2007**, *8*, 633.
[24] R. B. Borgens, E. Roederer, M. J. Cohen, *Science* **1981**, *213*, 611.
[25] J. A. Genovese, C. Spadaccio, H. G. Rivello, Y. Toyoda, A. N. Patel, *Cytotherapy* **2009**, *11*, 448.
[26] K. Ghosh, D. E. Ingber, *Adv. Drug Deliv. Rev.* **2007**, *59*, 1306.
[27] C. D. McCaig, A. M. Rajnicek, B. Song, M. Zhao, *Physiol. Rev.* **2005**, *85*, 943.
[28] N. C. Nowlan, P. Murphy, P. J. Prendergast, *J. Biomech.* **2008**, *41*, 249.
[29] G. A. Rodan, L. A. Bourret, L. A. Norton, *Science* **1978**, *199*, 690.
[30] L. A. MacGinitie, Y. A. Gluzband, A. J. Grodzinsky, *J. Orthop. Res.* **1994**, *12*, 151.
[31] N. S. Hwang, S. Varghese, H. J. Lee, Z. Zhang, Z. Ye, J. Bae, L. Cheng, J. Elisseeff, *Proc. Natl. Acad. Sci. USA* **2008**, *105*, 20641.